AGU PUBLICATIONS

JGR

Journal of Geophysical Research: Atmospheres

RESEARCH ARTICLE
10.1002/2014JD022604

Key Points:
- Surface energy balance of an Antarctic ice shelf examined in three models
- Significant biases found in radiative fluxes
- Results indicate need to improve albedo and cloud microphysics parameterizations

Correspondence to:
J. C. King,
jcki@bas.ac.uk

Citation:
King, J. C., A. Gadian, A. Kirchgaessner, P. Kuipers Munneke, T. A. Lachlan-Cope, A. Orr, C. Reijmer, M. R. van den Broeke, J. M. van Wessem, and M. Weeks (2015), Validation of the summertime surface energy budget of Larsen C Ice Shelf (Antarctica) as represented in three high-resolution atmospheric models, *J. Geophys. Res. Atmos.*, *120*, doi:10.1002/2014JD022604.

Received 19 SEP 2014
Accepted 28 JAN 2015
Accepted article online 1 FEB 2015

Validation of the summertime surface energy budget of Larsen C Ice Shelf (Antarctica) as represented in three high-resolution atmospheric models

J. C. King[1], A. Gadian[2], A. Kirchgaessner[1], P. Kuipers Munneke[3], T. A. Lachlan-Cope[1], A. Orr[1], C. Reijmer[3], M. R. van den Broeke[3], J. M. van Wessem[3], and M. Weeks[4]

[1]British Antarctic Survey, Cambridge, UK, [2]National Centre for Atmospheric Science, University of Leeds, Leeds, UK, [3]Institute for Marine and Atmospheric Research, Utrecht University, Utrecht, Netherlands, [4]Met Office, Exeter, UK

Abstract We compare measurements of the turbulent and radiative surface energy fluxes from an automatic weather station (AWS) on Larsen C Ice Shelf, Antarctica with corresponding fluxes from three high-resolution atmospheric models over a 1 month period during austral summer. All three models produce a reasonable simulation of the (relatively small) turbulent energy fluxes at the AWS site. However, biases in the modeled radiative fluxes, which dominate the surface energy budget, are significant. There is a significant positive bias in net shortwave radiation in all three models, together with a corresponding negative bias in net longwave radiation. In two of the models, the longwave bias only partially offsets the positive shortwave bias, leading to an excessive amount of energy available for heating and melting the surface, while, in the third, the negative longwave bias exceeds the positive shortwave bias, leading to a deficiency in calculated surface melt. Biases in shortwave and longwave radiation are anticorrelated, suggesting that they both result from the models simulating too little cloud (or clouds that are too optically thin). We conclude that, while these models may be able to provide some useful information on surface energy fluxes, absolute values of modeled melt rate are significantly biased and should be used with caution. Efforts to improve model simulation of melt should initially focus on the radiative fluxes and, in particular, on the simulation of the clouds that control these fluxes.

1. Introduction

Over the past 50 years, the Antarctic Peninsula has been one of the most rapidly warming regions on Earth [*Turner et al*., 2005]. Associated with this warming, there have been major changes in the regional cryosphere. Most notably, some of the ice shelves fringing the eastern coast of the Antarctic Peninsula have retreated rapidly and, in some case, disappeared entirely [*Cook and Vaughan*, 2012]. While basal melting may play a role in controlling the viability of some ice shelves, such as those in the Amundsen Sea sector of Antarctica, it is generally believed that the major driver of ice shelf retreat in the eastern Antarctic Peninsula is the increased surface melt associated with rising near-surface air temperatures during the melt season [*Scambos et al*., 2000; *van den Broeke*, 2005]. The loss of ice shelves from the eastern Peninsula has led to an increase in the rate of discharge of grounded ice [*Rignot et al*., 2004], implying an increased contribution to sea level rise from ice loss in this region. Changes in ice shelf extent may also affect bottom water production [*Huhn et al*., 2008] and carbon uptake [*Peck et al*., 2009]. The loss of Antarctic Peninsula ice shelves thus has potential impacts outside the Antarctic region, and it is necessary to understand the processes controlling these changes in order to make soundly based estimates of future changes in the regional cryosphere.

Limited temperature records are available for the eastern side of the Antarctic Peninsula. Analysis of these records shows that summer warming trends on the east coast of the Peninsula are around 3 times as large as those on the west coast. Furthermore, summer temperatures on the east coast correlate strongly with the strength of the circumpolar westerly winds. *Marshall et al*. [2006] hypothesized that this pattern of regional climate variability was caused by the interaction of the circumpolar westerly winds with the steep mountain barrier of the Antarctic Peninsula. They suggested that strengthening westerly winds would lead to an increase in the occurrence and/or intensity of warm, downslope Föhn winds to the east of the mountains, which would increase surface melt rates over ice shelves in this region. This hypothesis was supported by studies using the Regional Atmospheric Climate Model (RACMO) at 14 km resolution [*van Lipzig et al*., 2008] and by observations of a downslope wind event made using an instrumented aircraft [*King et al*., 2008].

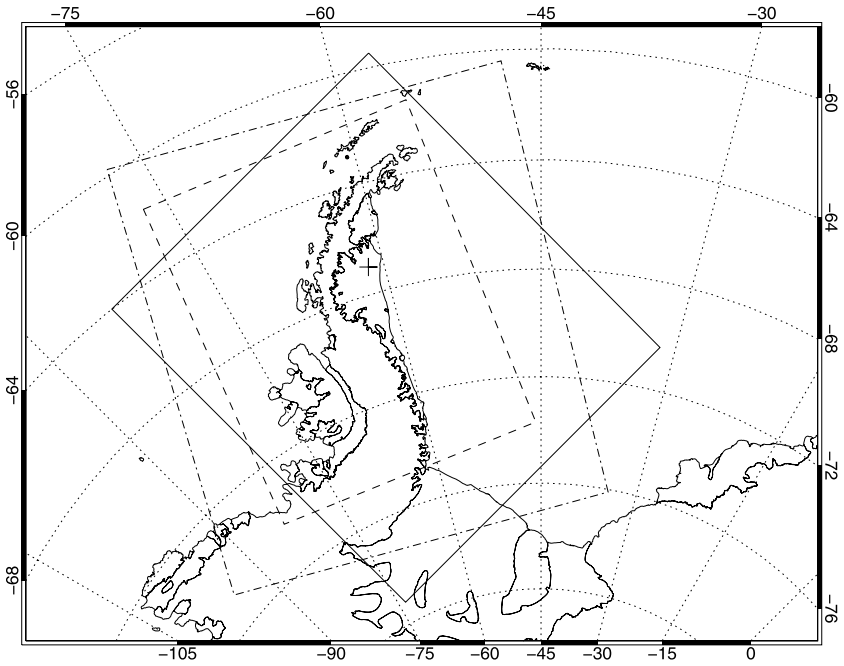

Figure 1. A map of the Antarctic Peninsula, showing the location of AWS14 (+) on Larsen C Ice Shelf. The domains of the 5 km AMPS model (solid line), the 4 km Unified Model (dashed line), and the 5.5 km RACMO2 model (dash-dotted line) are shown.

In order to understand the linkages between ice shelf stability and atmospheric circulation, it is necessary to study how the surface energy balance (and hence surface melt rate) on the ice shelves responds to changing atmospheric circulation. As direct measurements of surface energy balance and melt rates in this region are only available for a few locations and over limited time periods [*van den Broeke*, 2005; *Kuipers Munneke et al*., 2012], such studies are best carried out using high-resolution atmospheric models that are capable of representing the impact of the Antarctic Peninsula orography on the broad-scale flow and the subsequent interaction of the orographically modified flow with the ice shelf surface. Before using model output to study the climatology of surface energy balance, it is necessary to assess the ability of models to represent this quantity realistically. In this paper we compare estimates of the surface energy balance over Larsen Ice Shelf made using three high-resolution regional atmospheric models with measurements of the summertime surface energy balance from an automatic weather station.

2. Methods

2.1. Observations

Our focus is on the northern part of Larsen C Ice Shelf (Figure 1), the northernmost remaining significant ice shelf on the east coast of the Antarctic Peninsula. In January 2009, the Institute for Marine and Atmospheric Research, Utrecht University (IMAU) established an automatic weather station (henceforth referred to as AWS14) on Larsen C Ice Shelf at 67°00.8′S 61°28.8′W, elevation 40 m above sea level. The ice shelf surrounding the AWS is very flat and uniform. It extends approximately 100 km west of the AWS to the foot of the Antarctic Peninsula mountains and approximately 50 km east to the Weddell Sea coast. Measurements made at AWS14 are thus representative of a wide area. AWS14 measured air temperature and humidity, atmospheric pressure, wind speed and direction, and upwelling and downwelling fluxes of broadband longwave and shortwave radiation with sensors at a nominal height of 4 m above the snow surface. Additionally, the station was equipped with sensors to measure temperatures in the snowpack to 15 m depth. A full description of the sensors used and the corrections applied to the raw measurements is given by *Kuipers Munneke et al*. [2012]. During January 2011, a camp was established close to AWS14 and radiosondes were launched from this site at irregular intervals to record the structure of the troposphere over the ice shelf. A second set of radiation measurements was made at this camp, using similar sensors to those on AWS14 but with forced ventilation to minimize riming of the instruments. Mean differences in measured radiative fluxes between the two sets of instruments were less than

10 W m^{-2} for downwelling shortwave radiation and less than 3 W m^{-2} for downwelling longwave radiation, suggesting that riming of the AWS14 instruments was not a major contributor to measurement error.

The energy budget at the surface of a snowpack can be written as follows:

$$\mathrm{SW}\downarrow + \mathrm{SW}\uparrow + \mathrm{LW}\downarrow + \mathrm{LW}\uparrow + H_S + H_L = E \tag{1}$$

where SW↓ and SW↑ are, respectively, the downwelling and upwelling components of shortwave radiation, LW↓ and LW↑ are the downwelling and upwelling components of longwave radiation, H_S and H_L are, respectively the turbulent fluxes of sensible and latent heat, and E is the net surface energy flux available for heating, cooling, or melting the snowpack. We use the sign convention that energy fluxes directed toward the snow surface are positive, so a positive value of E means that the surface layers of the snowpack are warming and/or melting. We further define the surface melt energy flux E_{melt} as follows:

$$E_{\mathrm{melt}} = \begin{cases} 0 & T_s < 0°\mathrm{C} \\ E & T_s = 0°\mathrm{C} \end{cases} \tag{2}$$

where T_s is the snow surface temperature. Note that E_{melt} is not necessarily an accurate proxy for the actual melt rate, as melting can take place below the surface even when surface temperatures are below freezing due to absorption of shortwave radiation within the upper few centimeters of the snowpack [*Kuipers Munneke et al*., 2012]. We define the net shortwave and longwave radiative fluxes and the net radiation as

$$\mathrm{SW}_{\mathrm{net}} = \mathrm{SW}\downarrow + \mathrm{SW}\uparrow \tag{3}$$

$$\mathrm{LW}_{\mathrm{net}} = \mathrm{LW}\downarrow + \mathrm{LW}\uparrow \tag{4}$$

$$R_{\mathrm{net}} = \mathrm{SW}_{\mathrm{net}} + \mathrm{LW}_{\mathrm{net}} \tag{5}$$

respectively, and the surface albedo, α as

$$\alpha = \left| \frac{\mathrm{SW}\uparrow}{\mathrm{SW}\downarrow} \right| \tag{6}$$

AWS14 was equipped with sensors to measure the four radiative flux components in (1) directly. The turbulent fluxes were calculated from bulk formulae, using measured values of air temperature, humidity and wind speed, and the snow surface temperature, which was calculated iteratively using a snowpack energy balance model driven by the observed and calculated energy fluxes as described by *Kuipers Munneke et al*. [2009]. We have used this calculated snow surface temperature to determine the occurrence of surface melt. Using these directly measured and calculated fluxes, a 30 min resolution time series of all six of the surface energy budget components on the left-hand side of (1) was produced.

Following calculation of surface fluxes, measured air temperature and humidity and wind speed were corrected to standard levels of 2 m and 10 m, respectively, for comparison with model output. The climatology of the surface energy budget at AWS14 and its response to varying meteorological conditions is discussed by *Kuipers Munneke et al*. [2012]. In this paper, we compare measurements of surface energy fluxes at AWS14 during January and early February 2011 with corresponding fluxes computed by the three high-resolution atmospheric models described below.

2.2. AMPS Model

The Antarctic Mesoscale Prediction System (AMPS) [*Powers et al*., 2012] is a numerical weather prediction (NWP) system for the Antarctic region, run operationally by the Mesoscale and Microscale Meteorology Division of the National Center for Atmospheric Research. AMPS is implemented using the Weather Research and Forecasting (WRF) atmospheric model and, in January 2011, used the nonhydrostatic WRF v3.0.1 with modifications to improve the representation of the surface energy balance over permanently ice-covered regions. This model configuration is referred to as Polar WRF [*Hines and Bromwich*, 2008]. AMPS uses the Rapid Radiative Transfer Model longwave radiation scheme and the Goddard shortwave radiation scheme. Surface fluxes are calculated using the Eta similarity scheme, based on Monin-Obukhov similarity theory. Cloud microphysical properties are calculated using the WRF single-moment class 5 scheme [*Hong et al*., 2004].

The model was run on a series of nested domains with 44 vertical levels between the surface and the model top (10 hPa), with the lowest level approximately 16 m above the surface and with 12 levels in the lowest 1 km. The outermost (45 km resolution, 220 × 290 points) domain covered Antarctica and much of the Southern Ocean. A nested 15 km resolution (442 × 418 points) domain covered the Antarctic continent and, within this, a 5 km resolution (346 × 301 points) domain covered the Antarctic Peninsula region.

Lateral boundary conditions for the outer (45 km) domain were taken from the Global Forecast System (GFS) 0.5° global NWP system run by the U.S. National Centers for Environmental Prediction and were updated every 6 h. Observations within the AMPS domain were assimilated using a 3-D variational data assimilation scheme. Two runs of the AMPS system were carried out every day, starting from GFS analyses valid at 0000 UTC and 1200 UTC. Forecasts on the 5 km Antarctic Peninsula grid were run to $T+36$ h for each of these initialization times.

2.3. Met Office Unified Model

The UK Met Office Unified Model (UM) configuration used in this study was a nonhydrostatic version of UM version 8.2 run on a 4 km resolution (288 × 360 points) domain covering the Antarctic Peninsula, with 70 vertical levels up to a height of 40 km. The lowest model level was at 2.5 m above the surface, and there were 16 model levels in the lowest 1 km. The model configuration was based on the operational UK 4 km regional forecast system but included dynamics modifications [*Orr et al*., 2014] to improve the simulation of gravity waves over the Antarctic Peninsula mountains. The model includes a comprehensive set of parameterizations for radiative transfer [*Edwards and Slingo*, 1996], subsurface and surface fluxes [*Best et al*., 2011], boundary layer turbulence [*Lock et al*., 2000], and mixed phase cloud microphysics [*Wilson and Ballard*, 1999] with enhancements to include more hydrometeor species.

The UM 4 km model was nested within the UK Met Office operational global forecast model (approximately 25 km horizontal resolution over midlatitudes) starting from the analysis fields and using 3-hourly updates to the lateral boundaries. Two runs per day were carried out using the UM 4 km forecast system over the period 9 January 2011 to 8 February 2011, starting from analyses at 0000 UTC and 1200 UTC and running out to the 48 h forecast.

2.4. RACMO2 Model

The Regional Atmospheric Climate MOdel, version 2 (RACMO2) combines the hydrostatic dynamical core of the High Resolution Limited Area Model with the physics package of the European Centre for Medium-range Weather Forecasts (ECMWF) Integrated Forecast System. RACMO2 has been specifically adapted for use over the Antarctic continent, by using a sophisticated multilayer snow model [*Ettema et al*., 2010], a prognostic scheme that calculates surface albedo [*Kuipers Munneke et al*., 2011], and a drifting snow routine [*Lenaerts et al*., 2012]. The newest version of RACMO, version 2.3, with updated turbulence schemes and cloud microphysics [*van Wessem et al*., 2014], was used.

For the domain encompassing the Antarctic Peninsula (Figure 1), a horizontal resolution of 5.5 km was used together with 40 levels in the vertical. The lowest model level was at 9.5 m above the surface, and there were 10 model levels in the lowest 1 km. At the lateral boundaries the model was forced by ECMWF Re-Analysis (ERA)-Interim data [*Dee et al*., 2011] for the period 1979–2013. Unlike AMPS and the UM, which were run as short-range forecast models starting from an analysis step, RACMO2 ran continuously, with boundary conditions updated from ERA-Interim every 6 h.

2.5. Validation Methodology

We validate components of the surface energy balance and near-surface meteorological variables derived from all three modeling systems against observations from AWS14 over the period 1200 UTC 9 January 2011 to 1800 UTC 8 February 2011. Forecasts are available from AMPS and the UM at 6-hourly intervals from initializations at 0000 and 1200 UTC each day. We have chosen to validate the $T+12$ and $T+18$ forecasts from each of these initializations, giving us a 6-hourly time series of model data through the validation period. Previous studies using data from AMPS indicate that the atmosphere in the 5 km model is fully adjusted to the high-resolution topography and land surface by the $T+12$ forecast [*Seefeldt and Cassano*, 2008; *Steinhoff et al*., 2009]. Data are also available at 6 h intervals from the continuous run of RACMO2.

Table 1. Mean Biases, Their Standard Deviations (SD), and Correlation Coefficients for Modeled 6-Hourly Values of Surface and Near-Surface Variables Validated Against Corresponding Measurements From AWS14

Variable	AWS Mean	Mean Bias (Model-AWS)			SD of Bias			Correlation Coefficient		
		AMPS	UM	RACMO2	AMPS	UM	RACMO2	AMPS	UM	RACMO2
p_s (hPa)	986.99	−0.53	−0.55	−0.49	1.11	1.09	1.37	0.99	0.99	0.99
T_a (K)	269.98	−0.89	0.45	0.16	2.38	2.06	2.12	0.54	0.62	0.57
T_s (K)	270.69	−0.97	−0.53	−0.96	2.45	2.40	2.14	0.70	0.77	0.72
q_a (g kg^{-1})	2.68	−0.01	0.22	0.12	0.46	0.45	0.41	0.52	0.64	0.58
ff_{10} (m s^{-1})	3.87	0.27	−0.11	−0.47	1.77	2.11	1.65	0.79	0.69	0.84

Model field data for AMPS and the UM were bilinearly interpolated to the location of AWS14. For RACMO2, model data were taken from the nearest grid point to AWS14. For all three models, the model surface elevation at the point where data were extracted was within 3 m of the actual surface elevation at AWS14. Model variables were then compared with observations from AWS14 at times corresponding to the model validation time.

The 1 month validation period used is quite short but appears to be representative of summer conditions at this site over a number of years. January 2011 (mean temperature −2.0°C) was the warmest January in the AWS14 record (2010–2014) but was only 1.0°C warmer than the coldest January (2012). SW↓ was below average (284 W m^{-2} cf. 291 W m^{-2}) in January 2011, while LW↓ was above average (282 W m^{-2} cf. 277 W m^{-2}). The opposite anomalies in the two radiative fluxes suggest that January 2011 may have been somewhat more cloudy than average. The mean 10 m wind speed in January 2011 (3.1 m s^{-1}) was a little below the January mean for 2010–2014 (3.5 m s^{-1}).

3. Results

3.1. Basic Meteorological Variables

Since sensible and latent heat fluxes in the models are parameterized using near-surface variables, it is instructive to examine how well these variables are forecast before validating the surface energy balance. The comparison of 6-hourly modeled values of surface and near-surface meteorological variables with corresponding observations from AWS14 is summarized in Table 1. All three models forecast surface pressure, p_s, at this location with a high degree of skill, suggesting that they all provide a good representation of the synoptic and mesoscale weather systems that affect the site. Two meter air temperature, T_a, 2 m water vapor mixing ratio, q_a, and 10 m wind speed, ff_{10}, are also forecast with considerable skill, suggesting that all three models should be capable of realistic forecasts of the turbulent fluxes.

Surface temperature, T_s, is a key variable as it determines the onset of melt. All three models exhibit a small (≤1 K) overall cold bias in T_s. However, restricting attention to temperatures around melting point ($T_s = 0$°C) reveals differences between the models. Table 2 shows, for each model, the number of occasions (6-hourly forecasts) on which melt was both modeled and observed, those on which melt was modeled but not observed, and those on which melt was observed but not modeled. The UM significantly overpredicts the occurrence of melt (42 occurrences modeled against 18 observed), while RACMO2 underpredicts its occurrence (only 7 occurrences modeled against 18 observed). AMPS overpredicts the occurrence of melt but not to as larger degree as does the UM.

Table 2. Frequency of Occurrence (Number of 6-Hourly Predictions) of Surface Melt ($T_s = 0$°C) in Each of the Models Compared to Observations[a]

Model	Melt Modeled and Observed	Melt Modeled but Not Observed	Melt Not Modeled but Observed
AMPS	12	14	6
UM	18	24	0
RACMO2	5	2	13

[a]A total of 18 melt events were observed.

Table 3. Mean Biases in the Modeled Components of the Surface Energy Balance, Their Standard Deviations (SD), and Correlation Coefficients Between Observed and Modeled Values[a]

Variable	AWS Mean	Mean Bias (Model-AWS)			SD of Bias			Correlation Coefficient		
		AMPS	UM	RACMO2	AMPS	UM	RACMO2	AMPS	UM	RACMO2
SW↓	265.0	56.3	−31.6	39.2	109.9	116.8	83.3	*0.31*	*0.23*	*0.22*
SW↑	−225.1	−32.0	41.0	−32.3	87.0	102.1	69.5	*0.23*	*0.16*	*0.21*
LW↓	279.8	−9.8	−7.0	−24.9	37.1	30.3	28.3	0.55	0.65	0.60
LW↑	−302.2	3.3	−2.0	−0.05	11.1	11.5	10.3	0.61	0.72	0.66
SW_{net}	39.9	24.4	9.4	6.9	28.3	22.4	23.6	0.49	0.40	*0.11*
LW_{net}	−22.4	−6.4	−6.3	−25.0	33.2	24.9	23.0	0.46	0.52	0.53
R_{net}	17.5	17.9	3.0	−18.1	23.5	21.5	21.6	0.55	0.52	0.58
H_s	−6.0	−4.8	5.9	7.1	14.7	9.0	8.7	0.51	0.40	*0.17*
H_L	−10.0	5.2	1.9	4.7	6.7	8.4	7.0	0.43	0.51	0.52
E	1.5	18.4	10.5	−6.3	21.9	16.7	19.3	0.43	0.57	0.56
E_{melt}	7.0	6.3	7.6	−3.7	25.1	17.9	18.0	*0.30*	0.61	0.40

[a]Mean biases and their standard deviations have been calculated from 6 h data while correlation coefficients were evaluated for daily means so that they measure model skill in representing day-to-day variability rather than skill in reproducing the mean diurnal cycle. Correlation coefficients in italics are not significant at the 5% level or better.

3.2. Surface Energy Balance—Mean Biases

In Table 3, we compare mean modeled values of the energy fluxes contributing to the surface energy balance (equation (1)) with corresponding values derived from measurements at AWS14. Over the period examined in this paper, SW_{net} was the only positive contribution to the mean surface energy budget, balanced by negative mean contributions from (in decreasing order of magnitude) LW_{net}, H_L, and H_s.

AMPS and RACMO2 both exhibit positive mean biases in SW↓, while this flux is negatively biased in the UM. Biases are also seen in SW↑ in all three models, which can be attributed partly to the biases in SW↓ but also to differences between the albedo used in the model and that observed. SW_{net} is positively biased in all three models, with the largest bias seen in AMPS. From (3) and (6), the bias in SW_{net} can be written as

$$SW_{net}^{mod} - SW_{net}^{obs} = \left(SW^{mod}\downarrow - SW^{obs}\downarrow\right)\left(1-\alpha^{mod}\right) + SW^{obs}\downarrow\left(\alpha^{obs}-\alpha^{mod}\right) \quad (7)$$

where the superscripts obs and mod refer to observed and modeled values, respectively. The first term on the right-hand side of (7) represents the bias in SW_{net} that can be attributed to the bias in modeled SW↓, while the second term represents the bias that can be attributed to the difference between modeled and observed albedo. Table 4 shows the bias in SW_{net} for each model broken down into these two contributions. The mean observed albedo at AWS14 was 0.85, which is close to the mean albedo simulated by the RACMO2 model. AMPS and the UM both use lower values of albedo than that observed, leading to overestimation of solar heating of the surface. AMPS exhibits the largest bias in SW_{net}, resulting from roughly equal contributions from its bias in SW↓ and its use of an unrealistically low albedo. The bias in SW_{net} in the UM is smaller than that in AMPS as a result of the mean negative bias in SW↓ in the UM. RACMO2 has the smallest bias in SW_{net}, which results entirely from its bias in SW↓.

Downwelling longwave radiation is negatively biased in all three models, with RACMO2 showing a significantly larger bias than the other two models. Biases in upwelling longwave radiation are small so LW_{net} exhibits a net negative bias in all three models. In AMPS, the positive bias in SW_{net} exceeds the

Table 4. Contributions to the Bias in Net Shortwave Radiation (Column 3) From the Bias in Downwelling Shortwave Radiation (Column 4) and the Difference Between Model and Observed Albedo (Column 4) for All Three Models[a]

Model	α^{mod}	$SW_{net}^{mod} - SW_{net}^{obs}$	$(SW^{obs}\downarrow - SW^{mod}\downarrow)(1-\alpha^{mod})$	$SW^{obs}\downarrow(\alpha^{obs}-\alpha^{mod})$
AMPS	0.80	24.3	11.3	13.3
UM	0.79	9.3	−6.6	15.9
RACMO2	0.85	6.9	5.9	0.0

[a]Albedos have been rounded to two decimal places so the sum of the contributions does not exactly equal the total bias.

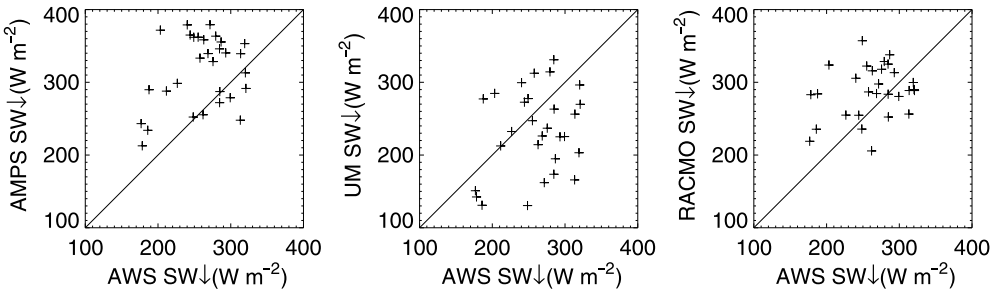

Figure 2. Modeled daily mean downwelling shortwave radiation, SW↓, plotted against measurements from AWS14 for (left) AMPS, the (middle) UM, and (right) RACMO2. The solid line indicates perfect agreement.

negative bias in LW_{net}, leading to a positive overall bias in net radiation in that model. In the UM, the biases in SW_{net} and LW_{net} almost exactly compensate so modeled mean net radiation agrees well with observations. In RACMO2, the negative bias in LW_{net} significantly exceeds the positive bias in SW_{net}, leading to a negative bias in net radiation.

Measurements from AWS14 show that mean values of the turbulent heat fluxes are somewhat smaller than the net radiative fluxes. The mean sensible and latent heat fluxes are both negative (directed upward), indicating the prevalence of convection at this site in summer. All three models exhibit small positive biases in H_L, while there is greater variability in the mean values of H_s from the models. While AMPS produces a mean negative H_s as observed, RACMO2 and the UM simulate small positive values.

The observed mean net energy flux, E, is small but is significantly positively biased in AMPS (as a result of the excessive net shortwave radiation in this model) and in the UM (as a result of positive biases in both turbulent heat fluxes). RACMO2 has a negative bias in E, reflecting the large negative bias in net longwave radiation in that model. Corresponding biases are seen in the mean melt energy flux, E_{melt}.

3.3. Surface Energy Balance—Temporal Variability

All three models simulate the diurnal cycle in SW↓ well (not shown) since it is largely determined by the diurnal variation in solar zenith angle. As we are principally interested in model performance on time scales longer than daily, we investigate the skill with which each of the three models simulates variability in the daily means of the components of the surface energy balance. Correlation coefficients between modeled and observed daily mean values of surface energy balance components are shown in Table 3, and scatterplots of modeled against observed components are shown in Figures 2–4.

None of the three models simulates day-to-day variations in SW↓ (Figure 2) with a great degree of skill. AMPS daily mean SW↓ is slightly better correlated with observations than that from the other two models, but recall that AMPS exhibits the greatest mean bias in this component. LW↓ variations (Figure 3) are better simulated than those in SW↓ by all three models. Variability in H_s (Figure 4) is quite well simulated by AMPS and the UM, but RACMO2 does not simulate the negative (i.e., upward) mean fluxes seen on many days.

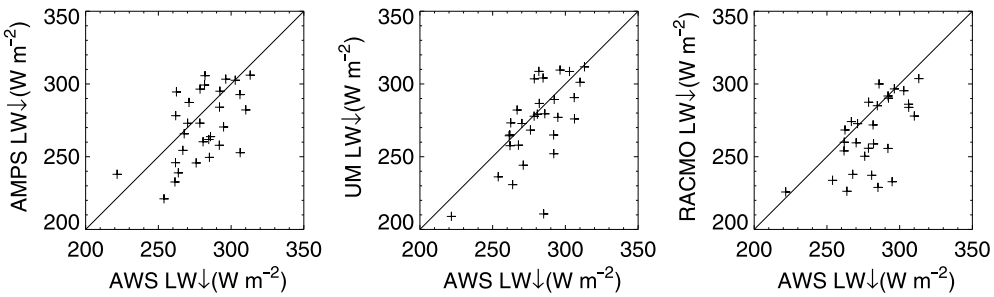

Figure 3. As in Figure 2 but for daily mean downwelling longwave radiation, LW↓.

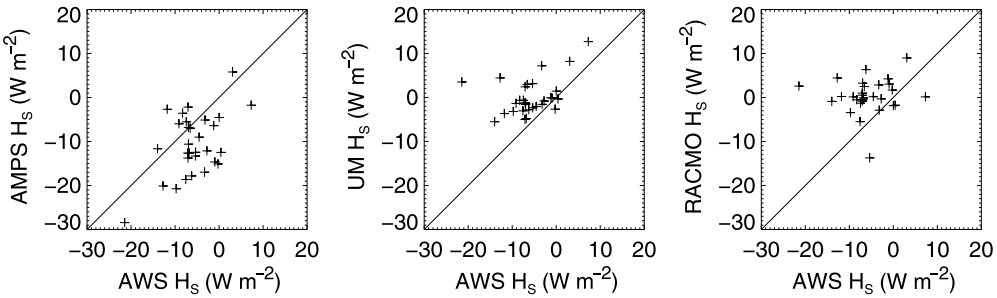

Figure 4. As in Figure 2 but for daily mean sensible heat flux, H_s.

This is consistent with the cold bias in surface temperature and infrequency of surface melt observed in RACMO2 (Tables 1 and 2). By contrast, variability in H_L (not shown) is simulated relatively well by all three models.

Day-to-day variability in the net surface energy flux, E (Figure 5) is simulated better by the UM and RACMO2 than by AMPS. For melt energy, E_{melt}, the UM exhibits higher skill than the other two models. The low correlation coefficient for RACMO2 E_{melt} (compared to that for E in the same model) clearly relates to the underprediction of surface melt by this model.

4. Discussion

Comparison of surface energy fluxes measured over Larsen C Ice Shelf in summer with modeled fluxes from the 5 km AMPS, the 4 km UM, and the 5.5 km RACMO2 models shows that each model has its strengths and weaknesses in simulating the mean values of the fluxes and their variability. The mean surface energy budget is dominated by the radiative fluxes, which exhibit significant biases in all three models. Downwelling shortwave radiation is positively biased in AMPS and RACMO2 but negatively biased in the UM. However, because AMPS and the UM simulate an unrealistically low surface albedo, net shortwave radiation is positively biased in all three models. All three models show only moderate skill in reproducing observed variations in shortwave radiation on time scales longer than daily.

The albedo parameterization used in RACMO2 is based on a prognostic equation for surface snow grain size and clearly produces more realistic results than the less sophisticated parameterizations used in the other two models. However, the representation of albedo in AMPS and the UM could easily be improved by using a "base" albedo (i.e., the albedo of freshly fallen snow) of 0.85 instead of the value of 0.8 currently used in these models.

The positive bias in net shortwave radiation is offset by a negative mean bias in net longwave radiation in all three models which results mostly from underprediction of the downwelling component, particularly in RACMO2. All three models show more skill in reproducing day-to-day variability in downwelling longwave radiation than that in shortwave radiation. Clouds, particularly those containing liquid water, become essentially opaque to longwave radiation at relatively low water contents, while their shortwave transmissivity continues to decrease with increasing water content. Hence, a realistic simulation of longwave

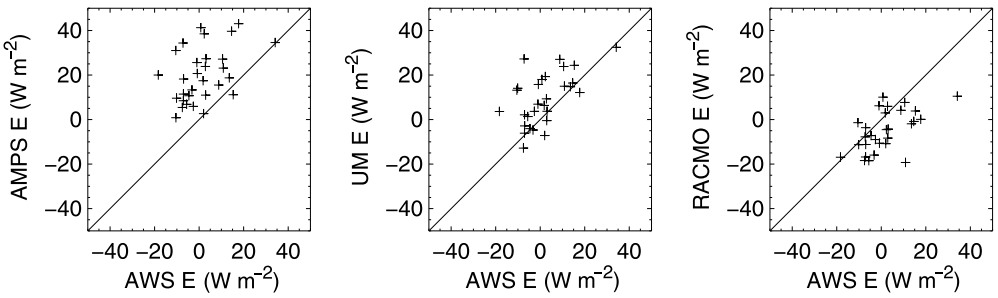

Figure 5. As in Figure 2 but for daily mean net surface energy flux, E.

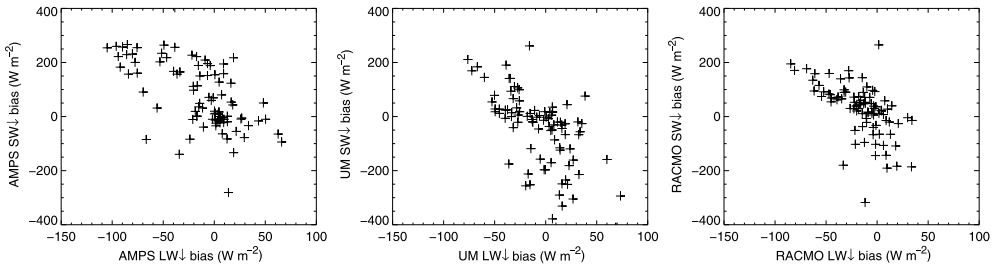

Figure 6. Six-hourly values of the bias in downwelling shortwave radiation against that in downwelling longwave radiation for (left) AMPS, (middle) the UM, and (right) RACMO2.

radiation may only require a good forecast of the presence or absence of cloud at a particular level, while accurate simulation of shortwave radiation also requires accurate simulation of cloud water content and microphysical properties.

Variability in the turbulent (sensible and latent) heat fluxes is simulated remarkably well by all three models although RACMO2 fails to capture some of the observed variability in sensible heat flux. Previous studies [e.g., *King and Connolley*, 1997; *Cassano et al*., 2001] have highlighted the difficulty of accurately simulating turbulent heat fluxes in the polar regions, but the present study suggests that the modern models studied here employ sufficiently realistic parameterizations and simulate the near-surface variables required to drive these parameterizations accurately enough to provide useful simulations of the fluxes. The mean biases in the simulated turbulent fluxes are of the same order of magnitude as the mean measured fluxes. However, averaged over the month studied, the mean turbulent fluxes are small and the biases do not contribute significantly to errors in the overall surface energy budget.

The mean surface energy budget is dominated by the radiative fluxes, which exhibit significant model biases. All three models have a positive bias in net shortwave radiation (significantly larger in AMPS than in the UM or RACMO2) and show only moderate skill in reproducing observed variations on time scales longer than daily. The shortwave bias is accompanied by a negative mean bias in net longwave radiation in all three models. The opposite signs of the biases in downwelling shortwave and longwave radiation in AMPS and RACMO2 suggest that, in these models at least, errors in the model simulation of clouds are the most likely source of these biases. Low clouds reduce downwelling shortwave radiation and increase downwelling longwave radiation (relative to clear skies), suggesting that both AMPS and RACMO2 are simulating a cloud fraction that is too low or clouds that are too optically thin in both the longwave and shortwave regions of the spectrum. The behavior of the UM is somewhat more complex. A negative bias in downwelling longwave radiation again suggests that the model is simulating cloud that is too optically thin in this region of the spectrum, while the negative bias in downwelling shortwave radiation suggests that model clouds have excessive optical thickness for shortwave radiation. Further evidence for the role of clouds in the biases comes from the observation (Figure 6) that individual 6-hourly values of the biases in downwelling shortwave radiation and downwelling longwave radiation are anticorrelated in all three models.

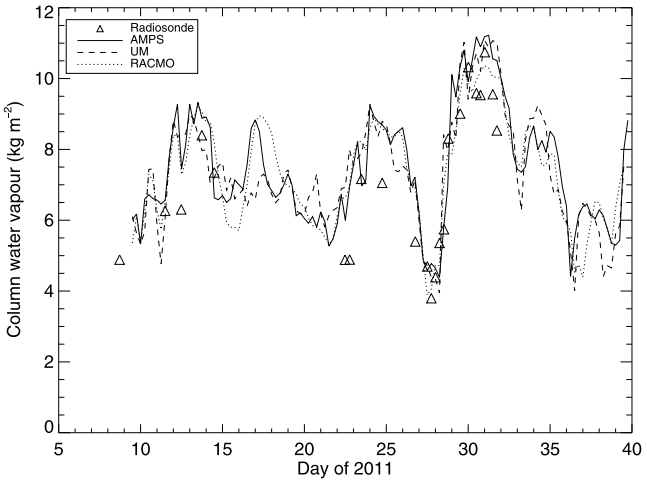

Figure 7. Total column water vapor as simulated by AMPS (solid line), the UM (broken line), RACMO2 (dotted line), and as measured by radiosondes launched from the location of AWS14 (triangles).

Models may represent clouds poorly either because of biases in the modeled fields of temperature and humidity or as

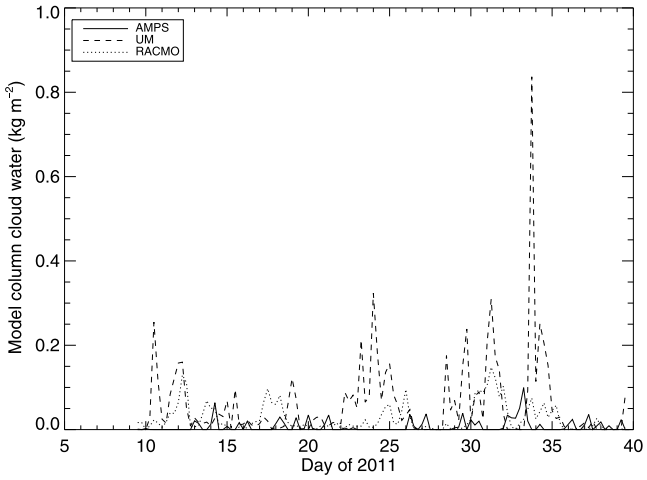

Figure 8. Total column cloud liquid water as simulated by AMPS (solid line), the UM (broken line), and RACMO2 (dotted line).

a result of inadequate parameterization of cloud microphysical processes. Figure 7 shows time series of modeled column water vapor from the three models plotted together with measurements of the same quantity from radiosondes launched from the camp at AWS14. The agreement between modeled and observed column water vapor is good, suggesting that model cloud biases are probably mostly due to inadequate parameterization of microphysics rather than poor representation of atmospheric humidity. Figures 8 and 9 show, respectively, time series of column cloud liquid water and cloud ice from all three models, and Table 5 gives mean values of these quantities. AMPS tends to simulate clouds that are predominantly of the ice phase, with very low (or even zero) liquid water. The UM, by contrast, simulates mixed phase clouds, with the liquid phase generally predominant and total condensate somewhat higher than that simulated by AMPS. RACMO2 simulates the lowest values of total condensate of all three models, producing clouds that are of mixed phase with a tendency for ice to predominate.

Visual observations of clouds from the camp at AWS14 made by one of the authors (P.K.M.) indicated cloud cover of 7/8 or greater for 69% of the time and 1/8 or less for only 3% of the time. By contrast, Figures 8 and 9 show that the models frequently forecast very low values of column liquid water and ice and hence probably forecast a much lower cloud fraction than that observed. The appearance of the observed clouds also suggested that, in contrast to those simulated by AMPS and RACMO2, they were predominantly composed of liquid water or were of mixed phase. *Grosvenor et al.* [2012] measured cloud water content and ice crystal concentrations in clouds over Larsen Ice Shelf during February 2010 using a Droplet Measurement Technologies Cloud Aerosol and Precipitation Spectrometer mounted on a Twin Otter aircraft. They reported that the observed clouds were mostly of mixed phase but that ice crystal concentrations were generally quite low. These observations suggest that the cloud microphysics schemes used by AMPS and RACMO2 are overpredicting the fraction of cloud water that is in the ice phase.

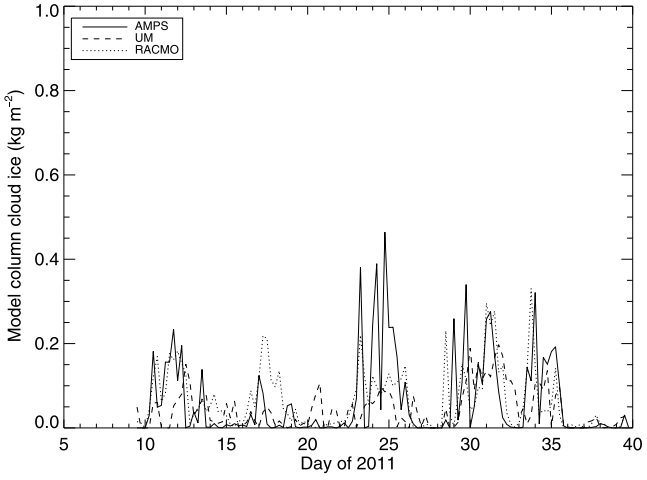

Figure 9. Total column cloud ice as simulated by AMPS (solid line), the UM (broken line), and RACMO2 (dotted line).

Figure 10 shows values of atmospheric shortwave transmissivity, $\tau_{SW} = SW\downarrow / SW_{toa}$, where SW_{toa} is the incoming shortwave radiation at the top of the atmosphere, for all three models as a function of total cloud condensate, q_{tot}. All three models give similar values for τ_{SW} under clear sky conditions ($q_{tot} = 0$), but the rate of decrease of τ_{SW} with increasing q_{tot} differs between the models. AMPS exhibits a relatively low rate of decrease, consistent with this model producing optically thin ice clouds, while the UM and RACMO2, which produce optically thicker mixed phase clouds, show a more rapid decrease of transmissivity with increasing cloud condensate. The large values of q_{tot} simulated by the UM lead

Table 5. Mean Values Over the Study Period of Column Cloud Liquid Water (q_{liq}), Column Cloud Ice (q_{ice}), and Column Total Cloud Condensate ($q_{tot} = q_{liq} + q_{ice}$) for All Three Models[a]

	AMPS	UM	RACMO2
q_{liq}	0.0079	0.0609	0.0148
q_{ice}	0.0623	0.0438	0.0341
q_{tot}	0.0702	0.1047	0.0489

[a]Units: kg m^{-2}.

to small values of transmissivity which will contribute to the negative bias in SW↓ seen in that model.

The sensitivity of modeled polar surface energy balance to the simulation of cloud properties has been noted before. *Wilson et al*. [2012] found biases in radiative fluxes simulated by Polar WRF over the Arctic of similar magnitude to those identified in this study. They showed that the biases were present even when the model correctly predicted the cloud cover, indicating that deficiencies in the parameterization of cloud microphysics and its interaction with radiation, rather than inadequate simulation of cloud fraction, were the primary cause of the bias. *Bromwich et al*. [2013] reached similar conclusions in a validation study of Polar WRF over the Antarctic. *Valkonen et al*. [2013] validated Polar WRF simulations of the surface energy balance over sea ice to the east of the Larsen Ice Shelf. As in the present study, they found a significant negative bias in LW↓ and observed that temporal variations in modeled cloud cover were poorly correlated with observations. *Van Wessem et al*. [2014] noted that simulations of Antarctic climate using RACMO2 were very sensitive to the cloud microphysics parameterization used. *Välisuo et al*. [2014] found biases in summertime radiative fluxes over Larsen Ice Shelf from three atmospheric reanalyses that were similar in both magnitude and sign to those found in the present study. Cloud microphysical parameterizations in atmospheric models are largely based on data gathered at low and middle latitudes and measurements of the microphysical properties of Antarctic clouds are limited [*Lachlan-Cope*, 2011]. Further measurements are urgently required to validate and improve the representation of clouds and their interaction with radiation in Antarctic regional models. All three models studied currently use relatively simple single-moment models for cloud microphysics, and it is not clear whether these models can adequately represent the mixed-phase cloud microphysical processes that characterize this region.

The mean surface melt energy flux, E_{melt}, derived from AWS14 observations corresponds to a mean melt rate of 1.8 mm water equivalent (mmwe) per day over the study period. The corresponding melt rates derived from the AMPS model (3.5 mmwe per day) and the UM (3.8 mmwe per day) are around double the observed rate, as a result of both the excessive net shortwave radiation and excessive frequency of melt predicted by the models. By contrast, the melt rate predicted by RACMO2 (0.9 mmwe per day) is only half of that observed. Although net shortwave radiation in RACMO2 is positively biased against observations, this is more than compensated for by a large negative bias in net longwave radiation. Furthermore, we have seen (Table 2) that RACMO2 significantly underpredicts the frequency of occurrence of melt. Taken together, these biases lead to a significant negative bias in the melt rate predicted by RACMO2.

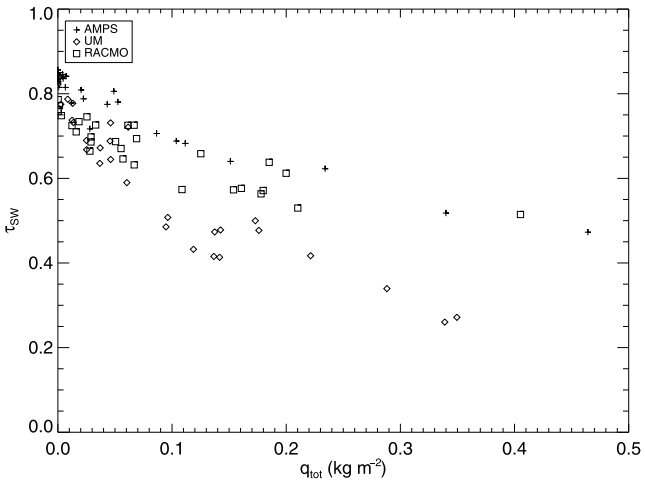

Figure 10. Atmospheric shortwave transmissivity as a function of column total cloud condensate for AMPS (cross), the UM (diamond), and RACMO2 (square). Points shown are for model data valid at 1800 UTC only to minimize the impact of varying solar zenith angle.

We conclude that care should be taken in interpreting absolute values of melt rates derived from any of these models. However, all models appear to exhibit a moderate degree of skill in simulating the day-to-day variability of surface energy fluxes (and hence the temporal variability in surface melt rates, if not their absolute values) over the period studied. To confirm that they can also provide useful information on surface energy balance and melt variability on seasonal and longer time scales will require extended model runs and longer validation data sets.

Our results indicate that efforts to improve model simulations of surface energy balance and melt should concentrate initially on reducing biases in modeled shortwave and longwave radiation. These biases both point to deficiencies in the representation of cloud properties in all three models examined here. The use of inappropriately low surface albedo values also contributes to net shortwave radiation biases in AMPS and the UM. Reducing these biases will require the development of improved surface albedo schemes and cloud microphysics parameterizations that are appropriate for the polar regions.

Acknowledgments

Data from AWS14 are available on request from IMAU, University of Utrecht (contact c.h.tijm-reijmer@uu.nl). Radiosonde observations from the AWS14 site may be obtained from the British Atmospheric Data Centre. AMPS model data are available through the Earth System Grid (www.earthsystemgrid.org). Data from the RACMO2.3 run used in this study are available on request from IMAU, University of Utrecht (contact m.r.vandenbroeke@uu.nl). Data from the 4 km Unified Model run (run reference xfkye) are archived at the UK Meteorological Office. The work reported in this paper was supported by the UK Natural Environment Research Council (NERC) under grant NE/G014124/1 "Orographic Flows and the Climate of the Antarctic Peninsula" and by the Netherlands Organisation for Scientific Research under grant 818.01.016. The IMAU AWS are funded by the Netherlands Polar Program (NPP) and the Netherlands Organization of Scientific Research, Earth and Life Sciences section (NWO/ALW). The UM simulations were carried out on the MONSooN supercomputer system, a collaborative facility supplied under the Joint Weather and Climate Research Programme, which is a strategic partnership between the UK Met Office and the NERC. We thank the Mesoscale and Microscale Meteorology Division of the National Center for Atmospheric Research for giving us access to the AMPS forecast archive, and the British Antarctic Survey staff at Rothera Research Station for supporting the field measurement program.

References

Best, M. J., et al. (2011), The Joint UK Land Environment Simulator (JULES), model description—Part 1: Energy and water fluxes, *Geosci. Model Dev.*, *4*(3), 677–699, doi:10.5194/gmd-4-677-2011.

Bromwich, D. H., F. O. Otieno, K. M. Hines, K. W. Manning, and E. Shilo (2013), Comprehensive evaluation of polar weather research and forecasting model performance in the Antarctic, *J. Geophys. Res. Atmos.*, *118*, 274–292, doi:10.1029/2012JD018139.

Cassano, J. J., T. R. Parish, and J. C. King (2001), Evaluation of turbulent surface flux parameterizations for the stable surface layer over Halley, Antarctica, *Mon. Weather Rev.*, *129*(1), 26–46.

Cook, A. J., and D. G. Vaughan (2012), Overview of areal changes of the ice shelves on the Antarctic Peninsula over the past 50 years, *Cryosphere*, *4*(1), 77–98.

Dee, D. P., et al. (2011), The ERA-Interim reanalysis: Configuration and performance of the data assimilation system, *Q. J. R. Meteorol. Soc.*, *137*(656), 553–597, doi:10.1002/qj.828.

Edwards, J. M., and A. Slingo (1996), Studies with a flexible new radiation code. I: Choosing a configuration for a large-scale model, *Q. J. R. Meteorol. Soc.*, *122*(531), 689–719, doi:10.1002/qj.49712253107.

Ettema, J., M. R. van den Broeke, E. van Meijgaard, and W. J. van de Berg (2010), Climate of the Greenland ice sheet using a high-resolution climate model—Part 2: Near-surface climate and energy balance, *Cryosphere*, *4*(4), 529–544, doi:10.5194/tc-4-529-2010.

Grosvenor, D. P., T. W. Choularton, T. Lachlan-Cope, M. W. Gallagher, J. Crosier, K. N. Bower, R. S. Ladkin, and J. R. Dorsey (2012), In-situ aircraft observations of ice concentrations within clouds over the Antarctic Peninsula and Larsen Ice Shelf, *Atmos. Chem. Phys.*, *12*(23), 11,275–11,294, doi:10.5194/acp-12-11275-2012.

Hines, K. M., and D. H. Bromwich (2008), Development and testing of polar Weather Research and Forecasting (WRF) Model. Part I: Greenland ice sheet meteorology, *Mon. Weather Rev.*, *136*(6), 1971–1989.

Hong, S.-Y., J. Dudhia, and S.-H. Chen (2004), A revised approach to ice microphysical processes for the bulk parameterization of clouds and precipitation, *Mon. Weather Rev.*, *132*(1), 103–120, doi:10.1175/1520-0493(2004)132<0103:aratim>2.0.co;2.

Huhn, O., H. H. Hellmer, M. Rhein, C. Rodehacke, W. Roether, M. P. Schodlok, and M. Schröder (2008), Evidence of deep- and bottom-water formation in the western Weddell Sea, *Deep Sea Res., Part II*, *55*, 1098–1116.

King, J., T. Lachlan-Cope, R. Ladkin, and A. Weiss (2008), Airborne measurements in the stable boundary layer over the Larsen Ice Shelf, Antarctica, *Boundary Layer Meteorol.*, *127*(3), 413–428.

King, J. C., and W. M. Connolley (1997), Validation of the surface energy balance over the Antarctic ice sheets in the U.K. Meteorological Office Unified Climate Model, *J. Clim.*, *10*, 1273–1287.

Kuipers Munneke, P., M. R. van den Broeke, C. H. Reijmer, M. M. Helsen, W. Boot, M. Schneebeli, and K. Steffen (2009), The role of radiation penetration in the energy budget of the snowpack at Summit, Greenland, *Cryosphere*, *3*(2), 155–165.

Kuipers Munneke, P., M. R. van den Broeke, J. T. M. Lenaerts, M. G. Flanner, A. S. Gardner, and W. J. van de Berg (2011), A new albedo parameterization for use in climate models over the Antarctic ice sheet, *J. Geophys. Res.*, *116*, D05114, doi:10.1029/2010JD015113.

Kuipers Munneke, P., M. R. van den Broeke, J. C. King, T. Gray, and C. H. Reijmer (2012), Near-surface climate and surface energy budget of Larsen C Ice Shelf, Antarctic Peninsula, *Cryosphere*, *6*(2), 353–363, doi:10.5194/tc-6-353-2012.

Lachlan-Cope, T. (2011), Antarctic clouds, *Polar Res.*, *29*(2), 150–158.

Lenaerts, J. T. M., M. R. van den Broeke, S. J. Déry, E. van Meijgaard, W. J. van de Berg, S. P. Palm, and J. Sanz Rodrigo (2012), Modeling drifting snow in Antarctica with a regional climate model: 1. Methods and model evaluation, *J. Geophys. Res.*, *117*, D05108, doi:10.1029/2011JD016145.

Lock, A. P., A. R. Brown, M. R. Bush, G. M. Martin, and R. N. B. Smith (2000), A new boundary layer mixing scheme. Part I: Scheme description and single-column model tests, *Mon. Weather Rev.*, *128*(9), 3187–3199, doi:10.1175/1520-0493(2000)128<3187:anblms>2.0.co;2.

Marshall, G. J., A. Orr, N. P. M. van Lipzig, and J. C. King (2006), The impact of a changing Southern Hemisphere Annular Mode on Antarctic Peninsula summer temperatures, *J. Clim.*, *19*(20), 5388–5404.

Orr, A., T. Phillips, S. Webster, A. Elvidge, M. Weeks, S. Hosking, and J. Turner (2014), Met Office Unified Model high-resolution simulations of a strong wind event in Antarctica, *Q. J. R. Meteorol. Soc.*, *140*(684), 2287–2297, doi:10.1002/qj.2296.

Peck, L. S., D. K. A. Barnes, A. J. Cook, A. H. Fleming, and A. Clarke (2009), Negative feedback in the cold: Ice retreat produces new carbon sinks in Antarctica, *Global Change Biol.*, *16*(9), 2614–2623.

Powers, J. G., K. W. Manning, D. H. Bromwich, J. J. Cassano, and A. M. Cayette (2012), A decade of Antarctic science support through AMPS, *Bull. Am. Meteorol. Soc.*, *93*(11), 1699–1712, doi:10.1175/bams-d-11-00186.1.

Rignot, E., G. Casassa, P. Gogineni, W. Krabill, A. Rivera, and R. Thomas (2004), Accelerated ice discharge from the Antarctic Peninsula following the collapse of Larsen B Ice Shelf, *Geophys. Res. Lett.*, *31*, L18401, doi:10.1029/2004GL020697.

Scambos, T. A., C. Hulbe, M. Fahnestock, and J. Bohlander (2000), The link between climate warming and break-up of ice shelves in the Antarctic Peninsula, *J. Glaciol.*, *46*(154), 516–530.

Seefeldt, M. W., and J. J. Cassano (2008), An analysis of low-level jets in the Greater Ross Ice Shelf region based on numerical simulations, *Mon. Weather Rev.*, *136*(11), 4188–4205.

Steinhoff, D. F., S. Chaudhuri, and D. H. Bromwich (2009), A case study of a Ross Ice Shelf airstream event: A new perspective, *Mon. Weather Rev.*, *137*(11), 4030–4046.

Turner, J., S. R. Colwell, G. J. Marshall, T. A. Lachlan-Cope, A. M. Carleton, P. D. Jones, V. Lagun, P. A. Reid, and S. Iagovkina (2005), Antarctic climate change during the last 50 years, *Int. J. Climatol.*, *25*(3), 279–294.

Välisuo, I., T. Vihma, and J. C. King (2014), Surface energy budget on Larsen and Wilkins Ice Shelves in the Antarctic Peninsula: Results based on reanalyses in 1989–2010, *Cryosphere*, *8*, 1519–1538, doi:10.5194/tc-8-1519-2014.

Valkonen, T., T. Vihma, M. M. Johansson, and J. Launiainen (2013), Atmosphere–sea ice interaction in early summer in the Antarctic: Evaluation and challenges of a regional atmospheric model, *Q. J. R. Meteorol. Soc.*, *140*, 1536–1551, doi:10.1002/qj.2237.

van den Broeke, M. (2005), Strong surface melting preceded collapse of Antarctic Peninsula ice shelf, *Geophys. Res. Lett.*, *32*, L12815, doi:10.1029/2005GL023247.

van Lipzig, N. P. M., G. J. Marshall, A. Orr, and J. C. King (2008), The relationship between the Southern Hemisphere Annular Mode and Antarctic Peninsula summer temperatures: Analysis of a high-resolution model climatology, *J. Clim.*, *21*, 1649–1668.

van Wessem, J. M., C. H. Reijmer, J. T. M. Lenaerts, W. J. van de Berg, M. R. van den Broeke, and E. van Meijgaard (2014), Updated cloud physics in a regional atmospheric climate model improves the modelled surface energy balance of Antarctica, *Cryosphere*, *8*(1), 125–135, doi:10.5194/tc-8-125-2014.

Wilson, A. B., D. H. Bromwich, and K. M. Hines (2012), Evaluation of Polar WRF forecasts on the Arctic System Reanalysis Domain: 2. Atmospheric hydrologic cycle, *J. Geophys. Res.*, *117*, D04107, doi:10.1029/2011JD016765.

Wilson, D. R., and S. P. Ballard (1999), A microphysically based precipitation scheme for the UK meteorological office unified model, *Q. J. R. Meteorol. Soc.*, *125*(557), 1607–1636, doi:10.1002/qj.49712555707.